Percolative spin-dependent transport in mesoscopic epitaxial Fe plaquettes of tailored connectivity

S. K. Bose, R. Sharma, and R. C. Budhani*
Condensed Matter–Low Dimensional Systems Laboratory, Department of Physics, Indian Institute of Technology Kanpur, Kanpur-208016, India

(Received 20 May 2008; revised manuscript received 1 July 2008; published 4 September 2008)

Spin-dependent charge transport in a two-tier granular system consisting of mesoscopic Fe plaquettes over which silver nanospheres are dispersed is investigated. This system transits from a Coulomb blockade regime with a finite voltage threshold for charge flow to an infinitely connected network showing dynamic resistance as the area coverage by Ag is increased. The zero-bias conductance ($G_{V=0}$) of the system at low coverage is thermally activated with an energy U^* ($\simeq$33 meV) equivalent to the charging energy of the Ag spheres. The current-voltage curves in this regime show power-law scaling with $\xi \approx 2.2$. A small ($\approx$0.8%) but distinct low-field ($\approx$0.2 T) magnetoresistance establishes the spin dependence of the Coulomb energy U^*.

DOI: 10.1103/PhysRevB.78.115403 PACS number(s): 73.23.Hk, 75.70.−i, 72.15.Gd

I. INTRODUCTION

Electron transport in two-dimensional (2D) periodic and aperiodic arrays of metal islands separated by poorly conducting or insulating medium shows a variety of fascinating characteristics including Coulomb blockade, size quantization, hopping conductivity, and universal conductance fluctuations.[1–5] Depending on the interisland separation and island geometry, the transport also has elements of percolation, and the system can undergo insulator-to-metal (I-M) transition on fine-tuning of these geometrical parameters. The modeling of the spatiotemporal behavior of flow in such systems yields a universal scaling between the flow velocity and the driving force.[6,7] The electronic conduction in 2D structures acquires added significance if the islands are magnetically ordered, which brings in the importance of the inter- and intraisland spin polarized transport.[8] While the flow of current in three-dimensional (3D) granular systems consisting of ferromagnetic and nonmagnetic metal clusters dispersed in dielectric host has been addressed extensively,[9] work on 2D systems is limited primarily to quenched-condensed ultrathin films[8,10–14] or self-assembled dot superlattices,[15,16] which give the structure a partial 3D character.

In this paper we address voltage driven electron transport in a 2D array of microscopic iron plaquettes deposited epitaxially on MgO using stress controlled growth processes. The geometry of these magnetic plaquettes varies from square to multicornered islands whose connectivity has been tuned by filling the gaps with silver. This nonmagnetic metal leads to the formation of a two-tier mesoscopic structure spanning nanometer to submicron length scales. At a small filling fraction, the Ag forms nanospheres on inter- and intraplaquette surfaces, leading to a transport controlled by the charging energy of the spheres. In the vicinity of threshold (V_T) for conduction, the current I scales with voltage V as $I \sim (V/V_T - 1)^{\xi}$, with $\xi = 2.2$, which is in agreement with the measurements on 2D disordered arrays.[3,17] At a higher Ag filling, a microstructure consisting of a continuous percolating backbone is obtained, in which electron transport is found to be in excellent agreement with the prediction of the dynamic random resistor network (DRRN) model.[18] A pronounced thermally activated magnetoresistance (MR) seen in samples with the lowest Ag filling establishes exchange splitting of the charging energy. While the peak MR here ($\approx$0.8%) is smaller than that seen in Fe-Al_2O_3 granular films, where a value as high as 5% is reported,[19] it matches well with the data ($\sim$1%) on 10 nm Fe layer covered with 2 nm of Au.[20]

II. EXPERIMENT

We have grown plaquettes of Fe on [100] MgO surface using the technique of pulsed laser ablation. A KrF excimer laser was used to ablate Fe, Pt, and Ag targets in an all-metal seal chamber maintained at 10^{-1} mbar of ultrahigh purity N_2 buffer. An Fe layer with nominal thickness of $\sim$40 nm, followed by $\sim$3 nm of Pt, was deposited at 700 °C, at which all nitrides of Fe are unstable. The N_2 was then removed and the sample was quenched to 50 °C, followed by deposition of Ag.

Scanning electron microscopy (SEM) and θ–2θ x-ray-diffraction measurements performed at resolutions of $\approx$2 nm and $\approx$18 arc sec, respectively, brought out some illuminating aspects of the topography and metallurgy of these synthetic structures. The temperature dependence of electrical resistivity [$\rho(T)$] and MR was measured in a two-probe configuration on bridges of 10×50 μm^2 created by Ar^+ ion milling of the films through shadow masks. The magnetoresistance of the samples is defined as $(R - R_0)/R_0$, where R_0 is the zero-field resistance. The magnetic state of the samples was probed with a superconducting quantum interference device (SQUID) based magnetometer.

III. RESULTS AND DISCUSSION

The growth of a percolating epitaxial structure requires control of lattice mismatch between substrate and the material to be deposited along with control of vapor flux and the mobility of adatoms on the growing surface.[21] The lattice parameters of Fe and MgO are 2.87 and 4.22 Å, respectively. However, the {100} atomic plane of bcc Fe matches well with the {110} plane of MgO, on which the interatomic spacing is 2.98 Å (3.6% more than the lattice parameter of

Fe). The tensile strain resulting from this mismatch and the high kinetic energy of Fe adatoms on hot (≈700 °C) MgO surface combined with the inherently energetic laser plume are sufficient to suppress the Frank–van der Merwe layer-by-layer growth mode[22] and favor either the layer-plus-island[23] or the isolated-island growth,[20] known as Stranski-Krastanov (SK) and Volmer-Weber (VW) modes, respectively. We will see shortly that the VW growth process is favored in the present case.

The thin Pt layer (3 nm) of the base template of Fe (40 nm) wets the Fe islands uniformly as a result of reaction with few top layers to form a FePt phase as evidenced by x-ray diffraction. This magnetically hard intermetallic compound enhances dipolar interaction between the Fe plaquettes and also serves as an oxidation resistant layer. The microstructure of the template consists of nearly rectangular Fe plaquettes with average area of $\approx 5 \times 10^4$ nm^2, separated by ≈20 nm. The resistivity of such a structure diverges rapidly on lowering the temperature below 300 K, and can be suppressed by thin silver films with nominal thicknesses of 2, 5, and 8 nm deposited on top of the FePt/Fe mesoscopic structure. However, the negligible solubility of Ag in Fe (Ref. 24) favors the formation of Ag islands on top of the Fe plaquettes and in the interplaquette spaces. When the Ag thickness is low (2 nm), the islands are spherical with a tight size distribution which peaks at ≈20 nm, as seen in the high-resolution SEM micrograph in Fig. 1(a). The interplaquette nanospheres of Ag impart some electrical conductivity in the Fe film. However, the system remains below the percolation threshold for I-M transition as evident from the current-voltage (I-V) characteristics shown in Fig. 1(b), which become increasingly nonlinear on lowering the temperature. In fact, below ≈90 K a threshold voltage is required to initiate flow of current, indicating Coulomb blockade of charge transport through the system [see inset of Fig. 1(b)].

When the Ag thickness is gradually increased to 8 nm, the islands start coalescing to form bigger islands, which now have a flat geometry as seen in Figs. 1(c) and 1(e), with a concomitant enhancement of electrical connectivity between the Fe plaquettes. A drop in the threshold voltage for conduction as well as the reduced spread in the I-V curves taken at different temperatures are a result of this additional connectivity. For the sample with nominal Ag thickness of 8 nm, this spread in I-V curves actually disappears.

The electron transport in such 2D percolating systems depends on several competing energy scales involving temperature, electrostatic charging of disconnected islands, size quantization, and the degree of spin polarization if the islands are ferromagnetic. At large drives (large bias voltage), some of these energy scales become irrelevant.[9] We first consider the conductance (G) of our Ag-FePt/Fe two-dimensional structures in the limit of zero bias ($G_{V=0}$). The $G_{V=0}$ of the 2, 5, and 8 nm Ag samples drops by factors of 200, 20, and 2.5, respectively, on lowering the temperature from 90 to 10 K and its absolute value at 10 K changes from 8.5×10^{-8} to 2.3×10^{-3} e^2/h from the thinnest to the thickest Ag structure. From these observations it is clear that the 2 nm sample, with $G_{V=0}$ much lower than the quantum conductance ($e^2/h \approx 3.9 \times 10^{-5}$ Ω^{-1}), is well below the percolation threshold and its zero-bias conductance is governed by electrostatic charging energy. The sample with Ag thickness equal to 5 nm is close to the percolation threshold as evident from the relatively small $\Delta G_{V=0}$ on cooling from 90 to 10 K and also from SEM micrographs, where one sees filling of interplaquette spacing by Ag islands. The sample with 8 nm Ag thickness is clearly above the percolation threshold as larger clusters spanning across the electrodes are seen in the SEM images [Fig. 1(e)].

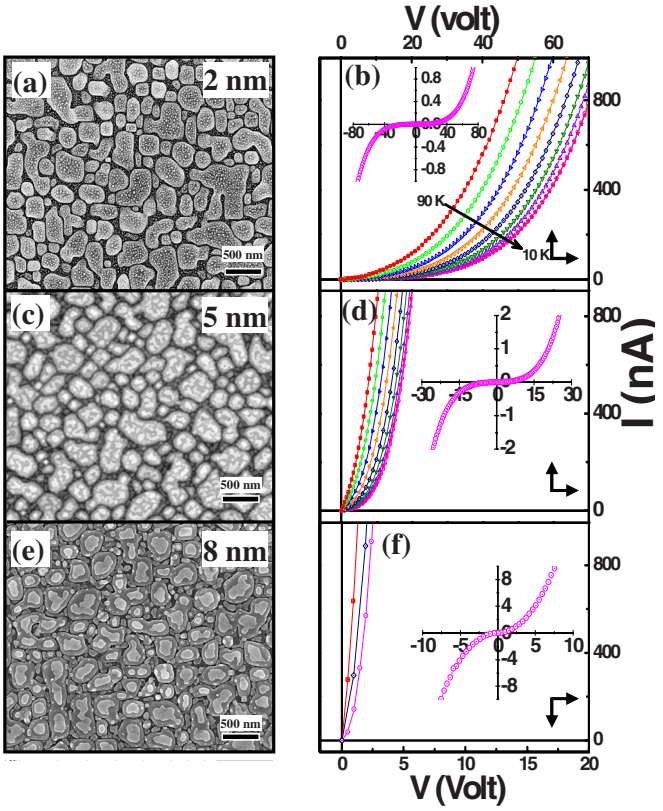

FIG. 1. (Color online) Panels (a), (c), and (e) respectively show SEM micrographs of the 2, 5, and 8 nm Ag capped FePt/Fe plaquettes deposited on (001) MgO. The Fe layer with nominal thickness of 40 nm was first grown at 700 °C followed by deposition of 3 nm Pt at the same temperature. The top silver layer was deposited at 50 °C. Panels (b), (d), and (f) show the first quadrant I-V characteristics of the corresponding samples measured at various temperatures in the range of 10–90 K. Please note that the voltage scales for (b) and (d) are the same (0–70 V), whereas for (f) the voltage varies from 0 to 20 V. The insets show the full I-V characteristics of the samples at 10 K, with the current given in microamperes.

We now consider the low-bias transport in the 2 nm sample, which can be visualized as a 2D disordered lattice of double tunnel junctions where electrons from Fe plaquettes tunnel into Ag nanodots and then tunnel forward onto another Fe plaquette. Each Fe mesostructure, however, has on average approximately eight neighbors to communicate to through the Ag islands. Since these plaquettes are not identical and the width of the interplaquette gap is also nonuniform, the simplest approach to understanding electron transport in such systems is the one pioneered by Abeles and co-workers[9] for granular metal films whose zero-bias conductance can be expressed as

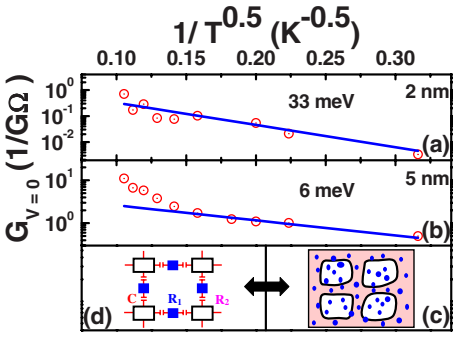

FIG. 2. (Color online) Plots of the zero-bias conductance $G_{V=0}$ vs $1/T^{0.5}$ for (a) 2 and (b) 5 nm Ag covered samples. The straight line is the fit to Eq. (1), where U^* can be identified with the Coulomb charging barrier. Appreciable deviation from this equation is seen in the case of the 5 nm sample at higher temperatures. Panel (c) presents a magnified representation of Fig. 1(a), where the four big Fe plaquettes and the interplaquette region are covered with smaller (blue) Ag islands. Panel (d) shows a simplified model for the two-tier granularity of this system. The conduction between Fe plaquettes (open rectangles) is mediated by a capacitative coupling with Ag islands (filled squares). Only four nearest neighbors of Fe plaquettes have been considered for clarity.

$$G_{V=0} \propto \exp(-\sqrt{U^*/k_B T}), \tag{1}$$

where U^* can be identified with the Coulomb charging barrier. In Figs. 2(a) and 2(b) we plot the dependence of $G_{V=0}$ on $T^{-1/2}$ for the 2 and 5 nm Ag samples, respectively. This yields a U^* of $\simeq$33 meV for the former and $\simeq$6.0 meV for the latter in the temperature range of 10–50 K. The calculated U^* for the 5 nm sample reflects the behavior of $G_{V=0}$ at the lower end of the temperature range as significant deviation from linearity is seen in the vicinity of 50 K.

If we consider the relevant charging energy (U^*) for the 2 nm sample, it comes to $\simeq$1 meV for Fe plaquettes ($\sim$250 nm diameter) and $\simeq$25 meV for Ag islands ($\sim$20 nm diameter). The U^* for the Fe structures was estimated by considering them to be $\sim$40 nm high circular pillars surrounded by approximately eight other pillars. For the spherical Ag islands, we have used $C \sim 2\pi\varepsilon_0\varepsilon_r \ln[(r+d)/d]$,[9] where r is the average island radius ($\sim$10 nm), $2d$ is the interparticle distance ($\sim$10 nm), and ε_r is the dielectric constant of tunnel barrier ($\approx$8 for MgO). The charging energy is then calculated by using $E_c \approx e^2/2C_{\rm nn}$, with $C_{\rm nn}=N_{\rm nn}C$ being the capacitance corrected for $N_{\rm nn}$ number of nearest neighbors. The U^* for Ag islands ($\simeq$25 meV) compares well with the calculated U^* ($\simeq$33 meV), suggesting thereby the dominant role of the finer structure in this two-tier mesoscopically disordered film, which can be represented as a network of capacitances (C) and resistances R_1 and R_2 as shown in Fig. 2(d). For the case of the 5 nm sample, the SEM reveals the very irregular shape and size of the Ag particles, which makes the calculation of charging energy highly inaccurate.

At low temperature ($k_B T \ll E_c$) and high electric fields (E), the potential difference between two neighboring metal grains (ΔV) exceeds E_c/e and the transport goes into a nonlinear regime, where the nonlinearity arises due to field-induced tunneling between isolated metal particles.[9] The

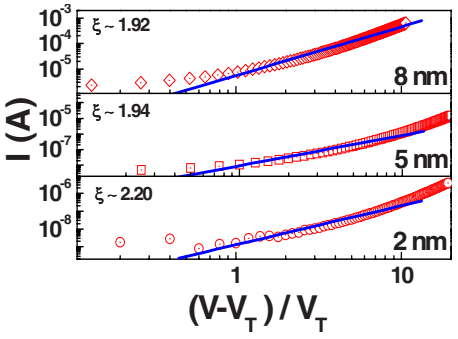

FIG. 3. (Color online) Plot of current (I) vs reduced voltage $[(V-V_T)/V_T]$ deduced from $I-V$ measurement performed at 10 K. For the bias voltage V greater than a threshold voltage (V_T), the current I shows a power-law dependence on the reduced voltage $[(V-V_T)/V_T]$ with a power ξ, which is equal to 2.20, 1.94, and 1.92 for the 2, 5, and 8 nm Ag covered samples, respectively. The exponent ξ has been extracted by fitting the data within the normalized voltage of 0.5–10.

drive-dependent transport in 2D arrays of metallic dots separated by insulating barriers was treated rigorously by Middleton and Wingreen.[6] The nonlinearity arises as more and more parallel current carrying channels open up between the electrodes with the increasing voltage. The current in the vicinity of threshold follows the scaling law $I \sim (V/V_T - 1)^{\xi}$, with $\xi=5/3$. In Fig. 3 we show the current ($\approx$ flow velocity) as a function of the bias voltage V ($\approx$ driving force) normalized with respect to the threshold voltage V_T for three samples of varying connectivities. For V/V_T in the range of 0.5–10, a power law with ξ=2.2, 1.94, and 1.92 for the 2, 5, and 8 nm samples, respectively, is inferred from these data. While for the ordered one-dimensional (1D) and 2D arrays of metal dots with ξ=1 and 5/3, respectively, in disordered arrays which are a better representative of the present situation, the exponent ξ monotonically increases from 1/2 to 2.0 as the system goes from 1D to 2D topography.[3,17] In 3D real systems, on the other hand, ξ exceeds 2.0. Numerical simulations of the flow in disordered systems also shows a drop in ξ at high driving forces.[7] This regime is never reached in our case. It is clear that while the charge flow in the 2 and 5 nm samples can be described on basis of the generalized models described in Refs. 6 and 7, we believe the physics of transport in the 8 nm Ag sample ($\xi \approx 1.92$) is quite different.

In this sample the diameter of Ag islands is bigger ($\sim$100 nm) than the mean separation between the Fe plaquettes [Fig. 1(e)]. Moreover, the silver also forms puddles on top of the Fe structures, thus leading to the absence of any voltage threshold in the I-V data [Fig. 1(f)]. Clearly, the transport in this system is beyond the scope of field-induced tunneling of charges between disconnected islands.[25] Since microscopic images of this sample show undisrupted conducting channels across the sample (infinite percolating backbone), we believe the DRRN model, in which the growth of conductance with driving force is due to a progressive transformation of insulating weak links to conducting channels, is applicable here. The model applies to conduction above the percolation threshold, $p > p_c$. In this regime, for sufficiently weak external current the I-V curves

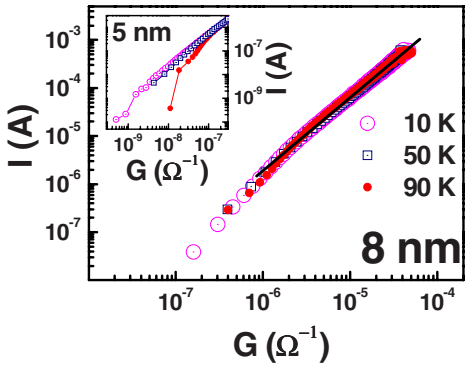

FIG. 4. (Color online) Plot of current (I) vs conductance (G) for the 8 nm Ag sample extracted from the I-V characteristics measured at 10, 50, and 90 K. A single universal dependence of G on I emerges at all temperatures. The slope of the linear part of the I vs G plot yields a dependence of the type $I \sim G^x$, with $x = 1.5 \pm 0.01$, in agreement with the DRRN model (Ref. 18). The inset of the figure shows a similar plot for the intermediate sample (5 nm), where dispersion in data points at higher temperatures indicates the absence of universal exponent x.

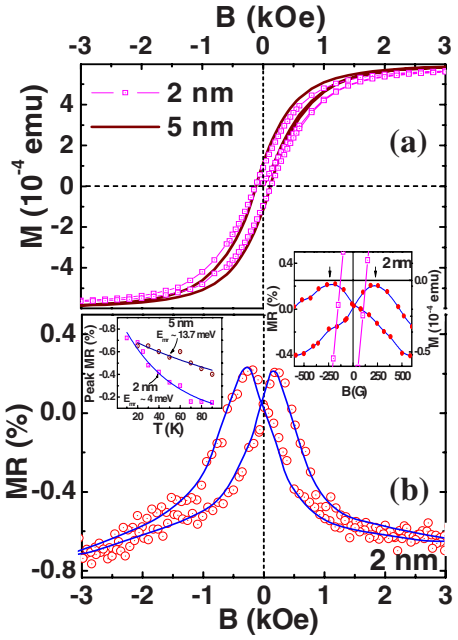

FIG. 5. (Color online) (a) Magnetization of the 2 and 5 nm Ag covered samples measured at 10 K. The data have been corrected for the linear diamagnetic contribution of the substrate. The loops are identical to each other with coercivity of ~130 Oe. Panel (b) shows the magnetoresistance of the 2 nm sample at 10 K. The peak in MR (at ~180 Oe) is at higher field compared to the coercive field measured by SQUID (~130 Oe) (see upper inset). The lower inset shows the temperature dependence of the peak magnetoresistance of the 2 and 5 nm samples. The solid line is a fit to $\exp(-k_B T/E_{MR})$. The characteristic energy E_{MR} is 4 and 13.7 meV for the 2 and 5 nm samples, respectively.

are linear and the conductance G goes to zero as $p \to p_c^+$. For 2D samples, this leads to a dependence of the type $I_c \sim G^x$, with $x \sim 1.5$,[18] where I_c is the critical current beyond which the response is nonlinear. To check whether a universal dependence of this type exists between current and conductance, in Fig. 4 we plot I vs G extracted from the I-V plots of the 8 nm sample in the temperature range of 10–90 K. Indeed, such a variation in G with I emerges at all temperatures. The slope of the linear part yields $x = 1.5 \pm 0.01$, in agreement with the theory. In the inset of Fig. 4 we show a similar plot of I vs G for the intermediate sample (5 nm Ag thickness). A scatter in the data is evident in the figure. Moreover the value of x in this case is only ≈ 1.32.

Now to check for the magnetic state of the nanoislands, we have measured the hysteresis loops with the in-plane magnetic field applied along the easy axis [100] of the film. The result of these measurements is shown in Fig. 5. All three samples with 2, 5, and 8 nm Ag overlayers show identical loops with saturation magnetization and coercivity of ≈ 2 kOe and ≈ 130 Oe, respectively. Figure 5 also shows the MR of the 2 nm sample with the in-plane magnetic field directed perpendicular to sample current. The MR saturates to -0.8% at ≈ 2 kOe when the moments of all Fe plaquettes become parallel, and is characterized by two peaks at ± 180 Oe on completing the field cycle. The position of these peaks is higher than the H_c (≈ 130 Oe) measured by SQUID. This discrepancy can be attributed to the fact that in the MR measurement the current samples only a fraction of the magnetic islands which fall on the percolating path, whereas the magnetization is a bulk measurement reflecting the average response of all Fe plaquettes. Nevertheless, the maximum in resistance in the vicinity of H_c where the sample is fully demagnetized, which will occur in this disconnected network of nearly single domain Fe plaquettes by antiferromagnetic interaction between the moments of neighboring plaquettes, shows that the tunneling process is inhibited. This indicates that the electron transport in the system is spin dependent. We have also examined how the MR evolves with temperature (T) and the role played by interplaquette silver in modulating its T dependence. These data, as shown in lower inset of Fig. 5, can be modeled as $\Delta R/R \propto \exp(-k_B T/E_{MR})$, where k_B is the Boltzmann constant and E_{MR} is a characteristic energy scale with values of ≈ 46 and ≈ 160 K for the 2 and 5 nm Ag samples, respectively. This energy is a measure of the exchange interaction and the cosine of the angle between the magnetization vectors of the two islands between which spin-dependent tunneling takes place at low bias voltages.[26] It is interesting to note that in these simple-metal-coupled 2D ferromagnetic plaquettes, the MR survives to higher temperature when the fraction of the former is increased. This behavior is in agreement with the observation of large room-temperature MR in inhomogeneous alloys Fe-Ag and Co-Cu.[27,28]

IV. CONCLUSIONS

In summary, we have studied the spin-dependent electronic transport in 2D films consisting of 40-nm-thick FePt/Fe plaquettes whose connectivity is varied by a Ag overlayer with nominal thicknesses of 2, 5, and 8 nm. High-resolution SEM reveals a two-tier granularity with characteristic lengths in micro- and nanometer scales. At the lowest

Ag thickness, the temperature and voltage-dependent charge transport shows signatures of spin-dependent Coulomb blockade, with thermal activation of $\simeq 33$ meV, which is comparable to the charging energy of a silver nanosphere ($\simeq 25$ meV) rather than that of an Fe plaquette ($\simeq 1$ meV). The current-voltage curves of the sample with low silver coverage show power-law scaling with exponent $\xi \approx 2.2$, in agreement with the result of numerical simulations on 2D disordered metal arrays. With higher silver coverage, the Coulomb blockade gives way to a nonthreshold regime with a dynamic, voltage-dependent resistance. Our experiments further establish that attractive two-dimensional mesoscale texture can be produced by stress and miscibility control during growth.

ACKNOWLEDGMENTS

This research was supported by grants from the Department of Science and Technology under its Nanoscience and Nanotechnology Initiative and by the Board for Research in Nuclear Science. S.K.B. acknowledges financial support from the Council for Scientific and Industrial Research, Government of India. The authors thank G. U. Kulkarni of JNCASR-Bangalore for facilitating the high-resolution SEM imaging of their samples.

*rcb@iitk.ac.in

[1] T. A. Fulton and G. J. Dolan, Phys. Rev. Lett. **59**, 109 (1987).
[2] E. Bar-Sadeh, Y. Goldstein, C. Zhang, H. Deng, B. Abeles, and O. Millo, Phys. Rev. B **50**, 8961 (1994).
[3] A. J. Rimberg, T. R. Ho, and J. Clarke, Phys. Rev. Lett. **74**, 4714 (1995).
[4] I. S. Beloborodov, A. V. Lopatin, and V. M. Vinokur, Phys. Rev. B **72**, 125121 (2005).
[5] P. A. Lee and A. D. Stone, Phys. Rev. Lett. **55**, 1622 (1985); P. A. Lee, A. D. Stone, and H. Fukuyama, Phys. Rev. B **35**, 1039 (1987).
[6] A. A. Middleton and N. S. Wingreen, Phys. Rev. Lett. **71**, 3198 (1993).
[7] C. Reichhardt and C. J. Olson Reichhardt, Phys. Rev. Lett. **90**, 046802 (2003).
[8] A. Frydman and R. C. Dynes, Solid State Commun. **110**, 485 (1999).
[9] P. Sheng, B. Abeles, and Y. Arie, Phys. Rev. Lett. **31**, 44 (1973); B. Abeles, P. Sheng, M. D. Coutts, and Y. Arie, Adv. Phys. **24**, 407 (1975).
[10] Y. M. Strelniker, R. Berkovits, A. Frydman, and S. Havlin, Phys. Rev. E **69**, 065105(R) (2004).
[11] K. R. Heim, G. G. Hembree, K. E. Schmidt, and M. R. Scheinfein, Appl. Phys. Lett. **67**, 2878 (1995).
[12] E. Navarro, Y. Huttel, C. Clavero, A. Cebollada, and G. Armelles, Phys. Rev. B **69**, 224419 (2004).
[13] K. Temst, M. J. Van Bael, and H. Fritzsche, J. Magn. Magn. Mater. **226-230**, 1840 (2001).
[14] Y. Xu, Z. G. Sun, Y. Qiang, and D. J. Sellmyer, J. Appl. Phys. **93**, 8289 (2003).
[15] C. T. Black, C. B. Murray, R. L. Sandstrom, and S. Sun, Science **290**, 1131 (2000).
[16] R. Parthasarathy, X.-M. Lin, and H. M. Jaeger, Phys. Rev. Lett. **87**, 186807 (2001).
[17] C. Kurdak, A. J. Rimberg, T. R. Ho, and John Clarke, Phys. Rev. B **57**, R6842 (1998).
[18] Y. Gefen, W.-H. Shih, R. B. Laibowitz, and J. M. Viggiano, Phys. Rev. Lett. **57**, 3097 (1986).
[19] T. Zhu and Y. J. Wang, Phys. Rev. B **60**, 11918 (1999).
[20] S. M. Jordan, R. Schad, A. M. Keen, M. Bischoff, D. S. Schmool, and H. van Kempen, Phys. Rev. B **59**, 7350 (1999).
[21] Y. Shiratsuchi, M. Yamamoto, and S. D. Bader, Prog. Surf. Sci. **82**, 121 (2007).
[22] T. Kanaji, K. Asano, and S. Nagata, Vacuum **23**, 55 (1973).
[23] G. Wedler, C. M. Schneider, A. Trampert, and R. Koch, Phys. Rev. Lett. **93**, 236101 (2004).
[24] M. Hansen and K. Anderko, *Constitution of Binary Alloys*, Suppl. 1 (McGraw-Hill, New York, 1958), pp. 20 and 580.
[25] O. Narayan and D. S. Fisher, Phys. Rev. B **49**, 9469 (1994).
[26] J. M. D. Coey, A. E. Berkowitz, Ll. Balcells, F. F. Putris, and A. Barry, Phys. Rev. Lett. **80**, 3815 (1998).
[27] A. E. Berkowitz, J. R. Mitchell, M. J. Carey, A. P. Young, S. Zhang, F. E. Spada, F. T. Parker, A. Hutten, and G. Thomas, Phys. Rev. Lett. **68**, 3745 (1992).
[28] J. Q. Xiao, J. S. Jiang, and C. L. Chien, Phys. Rev. Lett. **68**, 3749 (1992).